

# Toward $N$ to $N\pi$ matrix elements from lattice QCD

Lorenzo Barca,<sup>1,\*</sup> Gunnar Bali,<sup>1,†</sup> and Sara Collins<sup>1,‡</sup>

<sup>1</sup>*Fakultät für Physik, Universität Regensburg, Universitätsstr. 31, 93053 Regensburg, Germany*

(Dated: 28th March 2023)

QCD matrix elements of axial and vector currents between nucleons are required for the Monte Carlo reconstruction of the energy of neutrinos that are detected in long baseline oscillation experiments in the quasielastic regime. The cleanest approach for determining the axial matrix elements is lattice QCD. However, the extraction of these from the corresponding correlation functions is complicated by very large excited state contributions, that are related to transitions from the nucleon to a nucleon-pion pair. In this pilot study with a pion mass  $m_\pi = 429$  MeV, we demonstrate for the first time that these contributions can be removed by including five-(anti)quark operators into the basis of interpolators used to create the nucleon. The same techniques will be needed to compute transition matrix elements between the nucleon and nucleon-pion scattering states that are relevant in the resonance production regime.

## I. INTRODUCTION

The groundbreaking discovery of atmospheric and solar neutrino oscillations more than two decades ago by the Super-Kamiokande [1] and SNO [2] experiments, respectively, required an adjustment of the Standard Model to accommodate massive neutrinos. The present generation of terrestrial long baseline neutrino oscillation experiments, aimed at a more precise determination of the neutrino masses and mixing parameters, NOvA [3] and T2K [4] as well as the future DUNE [5] experiment and the upgrade of T2K to the Hyper-Kamiokande detector [6] determine the fluxes of muon and antimuon neutrinos via their interaction with nuclear targets in a near and a far detector. The neutrino energies of the scattering events are reconstructed via Monte Carlo event generators [7, 8], which require knowledge of the differential neutrino-nucleon cross section. For neutrino energies below 1 GeV this is dominated by (quasi-)elastic scattering, while from about 400 MeV onwards also resonance production with nucleon-pion ( $N\pi$ ) final states sets in [9]. Focusing on low energies, the cross section is proportional to the square of a combination of nonperturbative nucleon vector and axial matrix elements, which can be parameterized in terms of form factors. The two vector form factors as functions of the squared four-momentum transfer ( $Q^2$ ) are sufficiently well known from experiment. However, the two isovector axial form factors  $G_A(Q^2)$  and  $\tilde{G}_P(Q^2)$  are much less well constrained experimentally, apart from  $G_A$  in the forward limit ( $Q^2 = 0$ , i.e. the axial charge  $g_A$  [10]) and  $\tilde{G}_P(0.88 m_\mu^2) = g_P^*$  at the muon capture point of muonic hydrogen [11]. Fortunately, these form factors can be computed directly from QCD via lattice simulation. However, there is a tension [12, 13] between recent lattice results [14–18] and analyses of neutrino-deuteron scattering experiments [19]. Therefore, it is important

to establish the reliability of the lattice determinations. This requires the investigation of all systematics and, in particular, the one associated with extracting the nucleon matrix elements from correlation functions at finite Euclidean times. The latter receive contributions also from single- and multiparticle states with the same quantum numbers as the nucleon (normally referred to as excited states). At zero momentum, the lowest excitations with positive parity include  $N\pi$  P-wave and  $N\pi\pi$  S-wave scattering states, whereas, at nonvanishing momentum, parity is not a good quantum number and also  $N\pi$  in an S-wave can contribute. Towards small pion masses, the mass gap between the ground state and the first excitation decreases and the spectrum becomes more dense. Bearing in mind that the signal-to-noise ratio of correlation functions decreases exponentially with the Euclidean time separations, it can be very challenging to reliably extract nucleon matrix elements. In order to control the leading excited state contributions to these nucleon to nucleon form factors, we will, for the first time, explicitly calculate matrix elements that are also related to nucleon to  $N\pi$  transition form factors, which are required for a firm understanding of the resonance production regime.

Reliable continuum limit results for the axial form factors should reproduce the experimentally known values of  $g_A$  and  $g_P^*$  and also be consistent with the partially conserved axial current (PCAC) relation (also referred to as the axial Ward identity (AWI)), which relates the axial form factors to the pseudoscalar form factor. In many previous simulations  $g_A$  was reproduced, however,  $g_P^*$  (defined at  $Q^2 > 0$ ) was found to be smaller than the experimental value and also the AWI between form factors was significantly violated [16, 20–23]. Since the AWI was found to be satisfied on the level of the correlation functions in the continuum limit [24], the inconsistency had to be related to the difficulty of isolating the ground state contribution when extracting the form factors [14, 15, 24]. While the interpolator that is used to create the nucleon was found to have little overlap with excited states, as evidenced by analyses of two-point functions, transition matrix elements between different states, contributing to the spectral decomposition of the three-point function,

\* lorenzo.barca@desy.de

† gunnar.bali@ur.de

‡ sara.collins@ur.de

appeared to be enhanced. Indeed, in chiral perturbation theory (ChPT) the axial and pseudoscalar currents directly couple to the pion. Regarding the pseudoscalar current or the time-component of the axial current,  $N$  to  $N\pi$  transitions can contribute substantially to the three-point functions [25–27] (see also Refs. [28, 29]). At a small but nonvanishing momentum, the leading such contribution increases in proportion to the ratio of the nucleon mass over the pion energy,  $m_N/E_\pi$  [25, 26]. These terms were taken into account in recent analyses of the Euclidean time dependence of lattice correlation functions, where form factors were obtained, that are consistent with the AWI [14, 15, 17]. However, the size of the excited state contamination, found in these analyses, is quite large in some channels for the Euclidean times that are accessible at present. A more reliable approach would be to construct optimized interpolators to minimize the dominant ( $N\pi$ ) excited state contributions.

In this work, we take into account directly the  $N\pi$  contribution by constructing nucleon-pion-like interpolators  $[(qqq)(\bar{q}q)]$  with the quarks  $q \in \{u, d\}$   $O_{5q}$ , and computing the associated two-point and, for the first time, three-point correlation functions between the standard three-quark nucleon interpolator  $O_{3q}$  and  $O_{5q}$ . Using this basis, that has good overlap both with the nucleon ground state and the lowest lying  $N\pi$  state, nucleon to nucleon three-point functions can be constructed with minimized  $N\pi$  contributions, enhancing the reliability of the extraction of the nucleon matrix elements. As mentioned above, this is the first step towards determining nucleon to nucleon-pion matrix elements, associated with neutrino scattering in the resonance production regime [9, 13, 30]. In this pilot study we carry out the analysis for a single unphysical pion mass  $m_\pi = 429$  MeV. It turns out that even at this relatively large value the  $N\pi$  contribution is very significant and that this can effectively be removed with our approach. We expect this method to work even better at the physical pion mass: ChPT becomes more reliable as the pion mass is reduced, and the tree-level  $N\pi$  contribution is even more dominant, which is consistent with the observations made in Refs. [14, 15, 25–27].

## II. DEFINITION OF THE FORM FACTORS

We define local isovector pseudoscalar and axial currents,  $\mathcal{P} = \bar{d}\gamma_5 u$  and  $\mathcal{A}_\mu = \bar{d}\gamma_\mu\gamma_5 u$ , respectively. The Lorentz decompositions into form factors of the respective matrix elements read as

$$\langle n_{\mathbf{p}'} | \mathcal{P} | p_{\mathbf{p}} \rangle = \bar{u}_{\mathbf{p}'} G_P(Q^2) \gamma_5 u_{\mathbf{p}}, \quad (1)$$

$$\langle n_{\mathbf{p}'} | \mathcal{A}_\mu | p_{\mathbf{p}} \rangle = \bar{u}_{\mathbf{p}'} \left[ \gamma_\mu G_A(Q^2) + \frac{q_\mu}{2m_N} \tilde{G}_P(Q^2) \right] \gamma_5 u_{\mathbf{p}}, \quad (2)$$

where we assume isospin symmetry (i.e.  $m_N = m_p = m_n$  and  $m_\ell = m_u = m_d$  for the quark masses),  $u_{\mathbf{p}}$  is the spinor of a nucleon with three-momentum  $\mathbf{p}$ ,  $q_\mu = p'_\mu - p_\mu$  is the four-momentum transfer and  $Q^2 = -q_\mu q^\mu$ . Note

that the above decomposition of the axial matrix element does not hold if the two states differ in their mass, e.g., if a nucleon is on the right-hand side and a  $N\pi$  on the left. The AWI  $\partial_\mu \mathcal{A}^\mu = 2im_\ell \mathcal{P}$  implies the relation between form factors,  $m_N G_A(Q^2) = m_\ell G_P(Q^2) + (Q^2/4m_N) \tilde{G}_P(Q^2)$ , which is exact in the continuum limit but will be affected by moderate discretization effects at our lattice spacing  $a \approx 0.098$  fm [14, 24]. In addition, the pion pole dominance (PPD) assumption gives the approximate relation,  $\tilde{G}_P(Q^2) \approx 4m_N^2 G_A(Q^2)/(m_\pi^2 + Q^2)$ . While this only holds exactly for  $m_\pi = 0$ , in Ref. [14] it was found to hold within uncertainties of 1%–2% at the physical point in the continuum limit, with violations of less than 3% up to  $m_\pi \approx 420$  MeV. Deviations from these relations can be quantified in terms of the differences from unity of the combinations

$$r_{\text{PCAC}} = \frac{4m_N m_\ell G_P(Q^2) + Q^2 \tilde{G}_P(Q^2)}{4m_N^2 G_A(Q^2)}, \quad (3)$$

$$r_{\text{PPD}} = \frac{(m_\pi^2 + Q^2) \tilde{G}_P(Q^2)}{4m_N^2 G_A(Q^2)}. \quad (4)$$

## III. ANALYSIS

We construct the matrices of two- and three-point correlation functions (see the Supplemental Material),

$$C_{2pt}(\mathbf{p}, t)_{ij} = \langle O_i(\mathbf{p}, t) \bar{O}_j(\mathbf{p}, 0) \rangle, \quad (5)$$

$$C_{3pt}^{\mathcal{J}}(\mathbf{p}', t; \mathbf{q}, \tau)_{ij} = \langle O_i(\mathbf{p}', t) \mathcal{J}(\mathbf{q}, \tau) \bar{O}_j(\mathbf{p}, 0) \rangle, \quad (6)$$

where we indicate the three-momentum transfer in the argument of the local current  $\mathcal{J} \in \{\mathcal{P}, \mathcal{A}_\mu\}$ . The interpolators  $O_i \in \{O_{3q}, O_{5q}\}$  are projected onto the  $G_1$  representation of the double cover of the cubic group  ${}^2O_h$  (or, for nonvanishing momentum, the relevant little group) [31–33], corresponding to spin and helicity 1/2 in the continuum, as well as to definite momentum and isospin. For instance,  $I_3 = -1/2$  corresponds to  $O_{3q} \sim n$  and  $O_{5q} \sim \sqrt{1/3} n\pi^0 - \sqrt{2/3} p\pi^-$ . The Wick contractions of the correlation functions are evaluated using the sequential method [34] for quark-line connected topologies, while the stochastic “one-end-trick” [35–37] is used for disconnected diagrams.

For the results shown here, about 200 propagators (see the Supplemental Material) for each of the six source-sink separations have been computed on 800 gauge configurations. In view of the computational cost, we carry out the analysis on a single coordinated lattice simulations (CLS [38]) ensemble (A653, see Ref. [39]) with the spatial volume  $L^3 = (24a)^3$ , employing  $N_f = 3$  non-perturbatively improved Wilson fermions with a lattice spacing  $a \approx 0.098$  fm and the pion mass  $m_\pi = 429$  MeV. The best results were obtained, using extended (smeared) quark fields in the nucleon and pion interpolators. (For details on the smearing, see appendix C.1 and Table 15 of Ref. [39]).

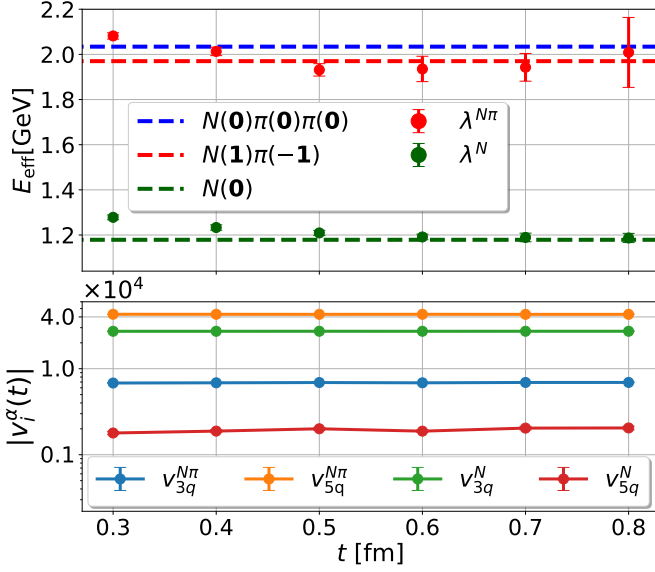


Figure 1. Top: the effective energies obtained solving the GEVP for  $\mathbf{p} = \mathbf{0}$  and  $t_0 = 0.2$  fm, compared with the nucleon mass and the lowest energy levels of noninteracting  $N\pi$  P- and  $N\pi\pi$  S-waves. Bottom: the moduli of the corresponding generalized eigenvector components.

We extract the generalized eigenvalue and eigenvector matrices  $\Lambda(\mathbf{p}, t; t_0) = \text{diag}(\lambda^1(\mathbf{p}, t; t_0), \lambda^2(\mathbf{p}, t; t_0))$  and  $V(\mathbf{p}, t, t_0) = (v^1(\mathbf{p}, t; t_0), v^2(\mathbf{p}, t; t_0))$ , respectively, by solving the generalized eigenvalue problem (GEVP) [40–43] for the matrix of two-point functions,  $C_{2pt}(\mathbf{p}, t)V(\mathbf{p}, t, t_0) = C_{2pt}(\mathbf{p}, t_0)V(\mathbf{p}, t, t_0)\Lambda(\mathbf{p}, t, t_0)$ , for fixed reference times  $t_0$ , where we employ the normalization  $v^{\alpha\dagger}C_{2pt}(t_0)v^\alpha = 1$ . For large times  $t$  the eigenvalues will decay exponentially with the energy of the state:  $\lambda^\alpha(\mathbf{p}, t; t_0) \rightarrow d^\alpha(\mathbf{p}; t_0)e^{-E^\alpha(\mathbf{p})(t-t_0)}$ , where  $d^\alpha \lesssim 1$ .

The effective energies  $E_{\text{eff}}^\alpha(t) = a^{-1} \ln[\lambda^\alpha(t)/\lambda^\alpha(t+a)]$  are shown in Fig. 1 for  $\mathbf{p} = \mathbf{0}$  and  $t_0 = 0.2$  fm. The lowest energy coincides with the nucleon mass on this ensemble [39], while the second level is close to the sum of the nucleon and pion energies for the lowest P-wave momentum combination. Therefore, we will identify  $N$  with  $\alpha = 1$  and  $N\pi$  with  $\alpha = 2$ . Note that the eigenvectors are very stable in  $t$  and that the contribution of  $O_{5q}$  (subscript  $i = 2$ ) to the nucleon state is suppressed by more than 1 order of magnitude relative to  $O_{3q}$ . Nevertheless, as we will see, the impact on three-point functions can be significant. We also solve the GEVP for moving frames, in particular for  $\mathbf{p} = \mathbf{e}_z = \frac{2\pi}{L}(0, 0, 1)$  ( $|\mathbf{e}_z| \approx 530$  MeV). Regarding  $O_{5q}$ , we consider the combinations  $O_{3q}(\mathbf{e}_z)O_{\bar{q}q}(\mathbf{0})$  and  $O_{3q}(\mathbf{0})O_{\bar{q}q}(\mathbf{e}_z)$ , with  $O_{\bar{q}q}$  being a pion interpolator. Solving the GEVP, in both cases we find the effective energy of the second eigenvalue for  $t > 0.5$  fm to be consistent with the  $N(\mathbf{e}_z)\pi(\mathbf{0})$  and  $N(\mathbf{0})\pi(\mathbf{e}_z)$  noninteracting energies, respectively.

Considering these results, we employ the generalized eigenvectors for  $t_0 = 0.2$  fm and  $t = 0.5$  fm to construct

the GEVP-optimized correlation functions,

$$C_{2pt}(\mathbf{p}, t)^\alpha = v_i^\alpha(\mathbf{p})C_{2pt}(\mathbf{p}, t)_{ij}v_j^\alpha(\mathbf{p}), \quad (7)$$

$$C_{3pt}^\mathcal{J}(\mathbf{p}', t; \mathbf{q}, \tau)^{\alpha\beta} = v_i^\alpha(\mathbf{p}')C_{3pt}^\mathcal{J}(\mathbf{p}', t; \mathbf{q}, \tau)_{ij}v_j^\beta(\mathbf{p}), \quad (8)$$

where  $\alpha, \beta \in \{N, N\pi\}$ . Note that here we only present results for  $\alpha = \beta = N$  and we neglect the  $i = j = 2$  element ( $5q$  to  $5q$ ) of  $C_{3pt}^\mathcal{J}$  that, in this case, is suppressed by the second power of the small eigenvector component  $v_{5q}^N$ . In addition, from ChPT we would only expect nondiagonal elements of the matrices of correlators to be enhanced. The nucleon matrix elements of interest are then extracted by forming the GEVP ratios [44–46]

$$R_\mathcal{J}(\mathbf{p}', t; \mathbf{q}, \tau) = \frac{C_{3pt}^\mathcal{J}(\mathbf{p}', t; \mathbf{q}, \tau)^{NN}}{C_{2pt}(\mathbf{p}', t)^N} \times \sqrt{\frac{C_{2pt}(\mathbf{p}', \tau)^N C_{2pt}(\mathbf{p}', t)^N C_{2pt}(\mathbf{p}, t - \tau)^N}{C_{2pt}(\mathbf{p}, \tau)^N C_{2pt}(\mathbf{p}, t)^N C_{2pt}(\mathbf{p}', t - \tau)^N}} \propto \langle N_{\mathbf{p}'} | \mathcal{J} | N_{\mathbf{p}} \rangle \quad (t \gg \tau \gg 0), \quad (9)$$

where excited state contributions of the type  $N \rightarrow N\pi$  and  $N\pi \rightarrow N$  are explicitly removed. Forming the same ratio for the usual two- and three-point functions,  $C_{2pt,11}$  and  $C_{3pt,11}^\mathcal{J}$ , will give the same result in the limit of large  $t$  and  $\tau$ . Any time dependence observed for these ratios (GEVP-improved or not) is an indication of remaining excited state contamination.

#### IV. RESULTS IN THE FORWARD LIMIT

For  $\mathbf{p}' = \mathbf{p}$  the combination under the square root in Eq. (9) cancels. We consider two kinematic combinations:  $\mathbf{p}' = \mathbf{p} = \mathbf{0}$  and  $\mathbf{p}' = \mathbf{p} = \mathbf{e}_z$ . Regarding the rest frame, the three-point functions vanish due to parity for  $\mathcal{J} = \mathcal{A}_4$  and  $\mathcal{J} = \mathcal{P}$ , while  $\mathcal{J} = \mathcal{A}_i$  (with the spin projected in the  $i$  direction) at large Euclidean time separations gives the axial charge  $g_A$ . Contamination from the coupling to  $N\pi$  states exists, however, only as a loop effect in ChPT. Indeed, even when using the standard ratio, for  $t > 0.8$  fm the data near  $\tau = t/2$  show no time dependence within their errors. Fitting the (unimproved) ratio for  $1.15 \text{ fm} < t < 1.4 \text{ fm}$ , we find  $g_A = 1.156(7)$  at our unphysical pion mass.

Also in the moving frame the  $N\pi$  contributions to  $\mathcal{A}_i$  only appear as loop effects, and we find that the corresponding standard ratio is almost constant (black stars in Fig. 2). However, regarding  $\mathcal{A}_4$  and  $\mathcal{P}$ ,  $N$  to  $N\pi$  transitions appear at tree-level and are enhanced by one power of  $m_N/E_\pi$ , relative to the  $N$  to  $N$  matrix elements of interest. The ratio  $R_{\mathcal{A}_4}$  will be proportional to  $g_A$  at large times too; however, using the  $O_{3q}$  interpolators, we find substantial excited state contamination, which is indicated by its strong dependence on the source-sink separation, see the blue symbols in the upper panel of Fig. 2. A difference between the ratios for  $\mathcal{A}_i$  and  $\mathcal{A}_4$  at  $\mathbf{p}' = \mathbf{p} \neq \mathbf{0}$  was also observed, e.g., in Ref. [47], using

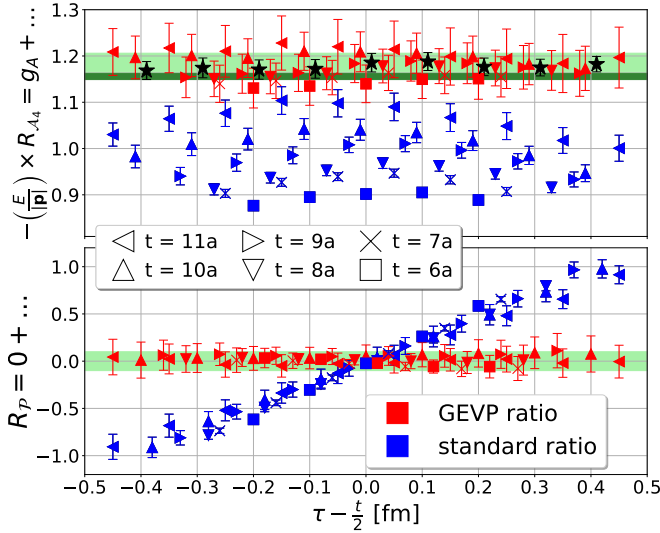


Figure 2. Comparison of the ratios in Eq. (9) in the forward limit, constructed from the standard and GEVP-optimized correlation functions, with  $\mathbf{p} = \mathbf{p}' = \mathbf{e}_z$  as a function of the current insertion time  $\tau$  for a number of different source-sink separations  $t$ , where  $a \approx 0.098$  fm. Top: renormalized ratio for the time component of the axial current. Also shown are the standard ratios for  $\mathcal{A}_z$  at  $\mathbf{p} = \mathbf{e}_z$  and  $t = 10a$  (black stars). The dark and light green bands correspond to  $g_A$ , extracted from this ratio at  $\mathbf{p} = \mathbf{0}$  and at  $\mathbf{p} = \mathbf{e}_z$ , respectively, using different  $t$ . Bottom: the same for the pseudoscalar current. The green band highlights the expected result.

standard interpolators. In contrast, the GEVP-improved ratios (red symbols) already agree for  $t > 0.6$  fm with the value extracted from the standard ratios for  $\mathcal{A}_z$  obtained at  $\mathbf{p} \neq \mathbf{0}$  (light green band) and at  $\mathbf{p} = \mathbf{0}$  (dark green band). A similar, dramatic reduction of the excited state contamination is observed for the pseudoscalar current for the GEVP-optimized correlation functions. For this current, due to charge conjugation symmetry, diagonal matrix elements vanish. Therefore, the deviation from zero of the standard ratio in the lower panel of Fig. 2 is entirely an excited state effect, which is removed within the present errors for the GEVP-optimized ratio. This demonstrates that the dominant contribution is from  $N$  to  $N\pi$  transitions, which is consistent with the tree-level ChPT expectation.

## V. RESULTS FOR NONVANISHING MOMENTUM TRANSFER

When determining the axial and pseudoscalar form factors, the excited state contamination is prominent for correlation functions involving the currents  $\mathcal{J} \in \{\mathcal{A}_4, \mathcal{P}\}$  [14, 25–27], that can transfer the momentum to a pion at tree-level in ChPT. This contribution, which is proportional to  $m_N/E_\pi$  [25, 26], is largest at small momentum transfer. Therefore, we consider these two currents and set  $\mathbf{q} = \mathbf{e}_z$  to a single unit of lattice momentum ( $|\mathbf{q}| \approx 530$  MeV). With  $\mathbf{p}' = \mathbf{0}$  and  $\mathbf{p} = -\mathbf{q}$ , this cor-

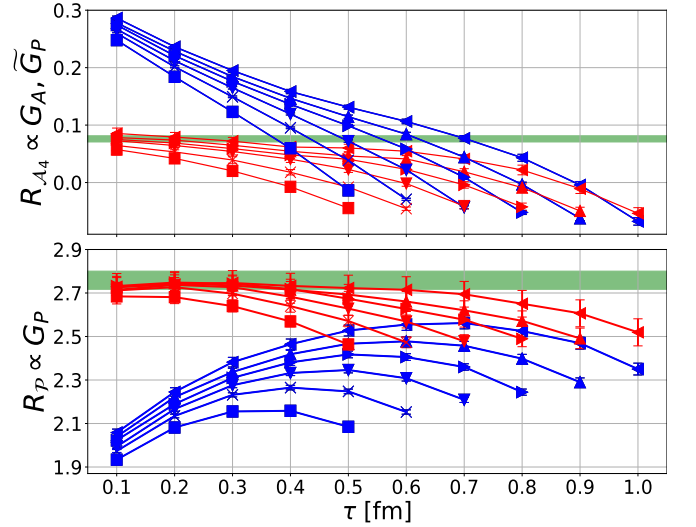


Figure 3. The same as in Fig. 2 (but as a function of the insertion time  $\tau$ ) for  $\mathbf{p}' = \mathbf{0} \neq \mathbf{p} = -\mathbf{e}_z$ , corresponding to  $Q^2 \approx 0.3$  GeV<sup>2</sup>. The green bands represent results of a simultaneous fit to the shown GEVP-optimized ratios and the standard ratio for  $\mathcal{A}_z$ .

responds to  $Q^2 \approx 0.3$  GeV<sup>2</sup>. Our results for the two ratios for the standard and optimized correlation functions are shown in Fig. 3. Clearly, the time dependence is much reduced for the GEVP-optimized results: at the source, excited states are effectively removed; however, at the sink (that is at rest) there are clearly residual effects from higher excitations. The ratios at large times (green bands) are proportional to the respective matrix elements which, using the decompositions (1) and (2), are related to a linear combination of  $G_A$  and  $\tilde{G}_P$  for  $\mathcal{A}_4$  and  $G_P$  for  $\mathcal{P}$ , respectively.

The axial form factor  $G_A = 0.91 \pm 0.01$  is extracted from the standard correlation functions with  $\mathcal{A}_i$  and  $\mathbf{e}_i \perp \mathbf{q}$ . These show ground state dominance within our range of  $t$  and  $\tau$ . Indeed, the large tree-level  $N\pi$  ChPT diagrams do not contribute to this channel and only  $N\pi$  loop diagrams appear [25]. The ground state matrix element is proportional only to  $G_A$  and we use the value we extract as a prior in fits to the other channels. We fit the GEVP-optimized ratios for the pseudoscalar and the temporal axial currents simultaneously to constants plus exponentials  $\propto e^{-\Delta E(t-\tau)}$ .

We find  $\Delta E \approx 2m_\pi$  for the gap between the nucleon ground state and this first excitation. The resulting matrix elements then give the pseudoscalar and induced pseudoscalar form factors at  $Q^2 \approx 0.3$  GeV<sup>2</sup>, the latter after subtracting the  $G_A$  contribution. The results for  $G_P$  and  $\tilde{G}_P$  as well as for the PCAC and PPD ratios of Eqs. (3) and (4) are shown in Fig. 4. We also include results that are obtained using the ChPT guided methods of Ref. [14] ( $M_1$ ) and a simultaneous fit to the channels  $\mathcal{A}_4$ ,  $\mathcal{P}$  and  $\mathcal{A}_i$  with  $\mathbf{q} = \mathbf{e}_i$ , inspired by [15] ( $M_2$ ). In spite of the large excited state contributions, the results

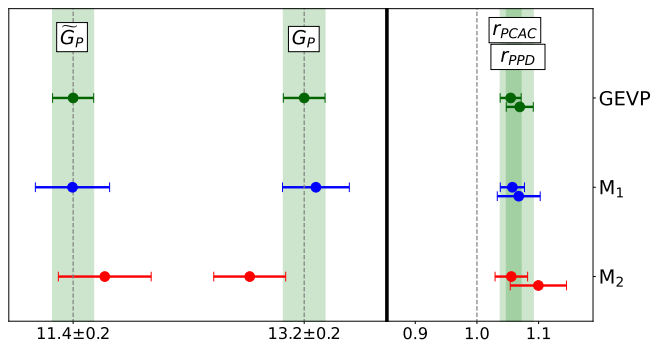


Figure 4. Results for the form factors and the PCAC and PPD ratios (3) and (4) at  $Q^2 \approx 0.3 \text{ GeV}^2$  from the GEVP-optimized correlators, in comparison to results obtained from the standard correlation functions, using the ChPT guided multistate analysis techniques of Ref. [14] ( $M_1$ ) and inspired by [15] ( $M_2$ ).

using modern multistate analysis techniques agree within errors with the GEVP results, at least at  $m_\pi = 429 \text{ MeV}$ . At this single lattice spacing, the ratio  $r_{\text{PCAC}}$  somewhat differs from 1.

## VI. CONCLUSIONS

Given the current tension [12, 13] between results for the axial form factor obtained from lattice QCD and from reanalyses of historical neutrino-deuteron scattering experiments [19], it is important to rigorously investigate the systematics associated with the lattice approach. The PCAC relation between form factors has only recently been verified in some studies [14, 15, 17] and this provides an important cross check. We have shown that the very large excited state contributions encountered can be removed by including  $N\pi$ -type interpolators. This confirms ChPT expectations, even at our relatively large pion mass, and supports assumptions made in recent determinations of the axial form factor [14–18]. In the near future, we will repeat the study at a smaller pion mass where excited state contributions are even larger, with the aim of also determining  $N$  to  $N\pi$  matrix elements that are relevant for the scattering of neutrinos with energies larger than 400 MeV.

## ACKNOWLEDGMENTS

The authors thank M. Göckeler, M. Padmanath, S. Prelovsek, P. Wein and T. Wurm for discussion. L.B. is grateful to G. Herdoiza for engaging discussions during his secondment to IFT Madrid and to A. Kronfeld, M. Wagman, W. Detmold and P. Shanahan for fruitful discussions and their hospitality at Fermilab and MIT. This project has received funding from the European Union’s Horizon 2020 research and innovation program under the Marie Skłodowska Grant Agreement No. 813942 (ITN EuroPLEx) and the EU Grant Agreement No. 824093 (STRONG 2020). Support from the MISTI Global Seed Fund MIT-Germany - University of Regensburg project “Quark and gluon structure of the proton” is gratefully acknowledged. The authors thank the Gauss Centre for Supercomputing (GCS) for providing computing time through the John von Neumann Institute for Computing (NIC) on the Booster partition of the supercomputer JURECA [48] at Jülich Supercomputing Centre (JSC). G. C. S. is the alliance of the three national supercomputing centres HLRS (Universität Stuttgart), JSC (Forschungszentrum Jülich), and LRZ (Bayerische Akademie der Wissenschaften), funded by the BMBF and the German State Ministries for Research of Baden-Württemberg (MWK), Bayern (StMWFK) and Nordrhein-Westfalen (MIWF). Simulations were also performed on the QPACE 3 computer of SFB/TR-55, using an adapted version of the CHROMA [49] software package.

## Supplemental Material

### CONSTRUCTION OF THE TWO- AND THREE-POINT FUNCTIONS

In order to employ the generalized eigenvalue (and eigenstate) approach, the following two-point correlation functions (see Eq. (5))

$$\langle O_{3q}(\mathbf{p}, t) \bar{O}_{3q}(\mathbf{p}, 0) \rangle, \quad (S1)$$

$$\langle O_{5q}(\mathbf{p}, t) \bar{O}_{3q}(\mathbf{p}, 0) \rangle, \quad (S2)$$

$$\langle O_{5q}(\mathbf{p}, t) \bar{O}_{5q}(\mathbf{p}, 0) \rangle \quad (S3)$$

and three-point correlation functions (see Eq. (6))

$$\langle O_{3q}(\mathbf{p}', t) \mathcal{J}(\mathbf{q}, \tau) \bar{O}_{3q}(\mathbf{p}, 0) \rangle, \quad (S4)$$

$$\langle O_{5q}(\mathbf{p}', t) \mathcal{J}(\mathbf{q}, \tau) \bar{O}_{3q}(\mathbf{p}, 0) \rangle \quad (S5)$$

need to be evaluated. In these expressions,  $O_{3q}$  represents a nucleon-like interpolating operator with a 3-quark  $qqq$  structure and  $O_{5q}$  is nucleon-pion-like with a  $(qqq)(\bar{q}q)$ -structure.

We first discuss the construction of the three-point functions, where we consider transitions from an  $I = I_3 = 1/2$  state (e.g., the proton  $p$ ) via a charged current  $\mathcal{J} = d\Gamma u$  to an  $I = -I_3 = 1/2$  state (e.g., the neutron,  $n$ ), i.e.  $\bar{O}_{3q}$  has the flavour structure  $\bar{u}\bar{u}\bar{d} \sim \bar{p}$ , whereas  $O_{3q}$  corresponds to  $udd \sim n$ . To project  $O_{5q}$  onto  $I = -I_3 = 1/2$ , the combination  $\sqrt{1/3}n\pi^0 - \sqrt{2/3}p\pi^-$  must be formed, where  $\pi^- \sim \bar{u}d$  and  $\pi^0 \sim 1/\sqrt{2}(\bar{u}u - \bar{d}d)$ . Like  $O_{3q}$  also  $O_{5q}$  must be projected onto the lattice irreducible representation  $G_1$ , see, e.g., Refs. [32, 33]. In the rest frame, for the spin-up component, we form the combination

$$\begin{aligned} O_{5q}^{G_1, \uparrow}(\mathbf{0}) = & O_{3q}(-\mathbf{e}_x)O_{\bar{q}q}(\mathbf{e}_x) - O_{3q}(\mathbf{e}_x)O_{\bar{q}q}(-\mathbf{e}_x) \\ & - iO_{3q}(-\mathbf{e}_y)O_{\bar{q}q}(\mathbf{e}_y) + iO_{3q}(\mathbf{e}_y)O_{\bar{q}q}(-\mathbf{e}_y) \\ & + O_{3q}(-\mathbf{e}_z)O_{\bar{q}q}(\mathbf{e}_z) - O_{3q}(\mathbf{e}_z)O_{\bar{q}q}(-\mathbf{e}_z), \end{aligned} \quad (S6)$$

where  $\mathbf{e}_i$  corresponds to one unit of lattice momentum in the  $i$ -direction and  $O_{\bar{q}q}$  is a pion interpolator. Regarding a moving frame with  $\mathbf{p}' = \mathbf{e}_z$ , we employ two combinations that, in the continuum limit, will project on the helicity  $+1/2$ :

$$O_{5q}^{G_1, \uparrow}(\mathbf{e}_z)^1 = O_{3q}^\uparrow(\mathbf{e}_z)O_{\bar{q}q}(\mathbf{0}), \quad (S7)$$

$$O_{5q}^{G_1, \uparrow}(\mathbf{e}_z)^2 = O_{3q}^\uparrow(\mathbf{0})O_{\bar{q}q}(\mathbf{e}_z). \quad (S8)$$

Following tree-level ChPT, in the forward limit ( $\mathbf{q} = \mathbf{0}$ ), in the moving frame ( $\mathbf{p} = \mathbf{p}' = \mathbf{e}_z$ ), Eq. (S7) is the

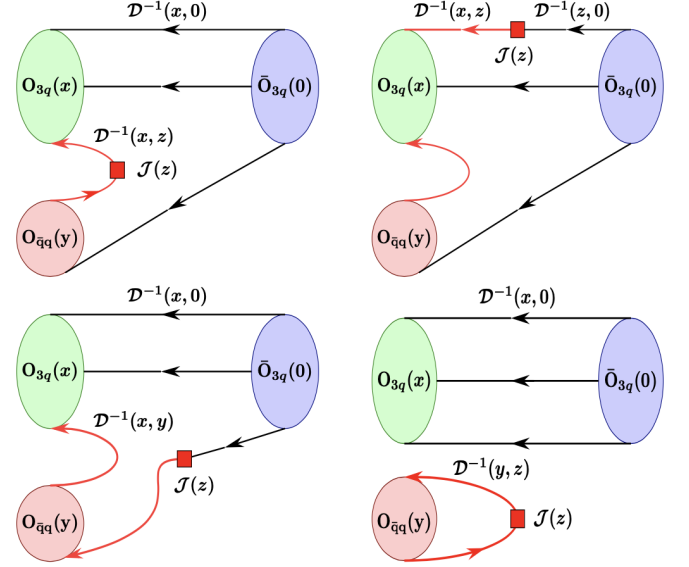


Figure S1. Topologies in position space that appear after performing the Wick contractions of the three-point correlation functions  $\langle O_{5q}(x, y) \mathcal{J}(z) \bar{O}_{3q}(0) \rangle$ . The three black lines represent point-to-all propagators, the two red lines correspond to all-to-all propagators and the red square indicates the current insertion at  $z = (\mathbf{z}, \tau)$ . The  $O_{5q}(x, y)$  interpolator contains a  $qqq$ -structure ( $O_{3q}(x)$ ) at the spacetime position  $x = (\mathbf{x}, t)$  and a  $\bar{q}q$ -structure ( $O_{\bar{q}q}(y)$ ) at  $y = (\mathbf{y}, t)$ .

relevant interpolator, while for off-forward kinematics ( $\mathbf{p}' = \mathbf{e}_z, \mathbf{p} = \mathbf{0}$ ) Eq. (S8) is used.

Performing the Wick contractions, we encounter the four different quark-line diagram topologies shown in Fig. S1. Each topology represents a number of different Wick contractions. Note that for the charged current we are interested in, the

disconnected diagram does not contribute to the transition  $p \rightarrow n\pi^0$ , whereas all four diagrams contribute to  $p \rightarrow p\pi^-$ . In each diagram there are two all-to-all propagators (red lines).

The quark-line disconnected diagram on the bottom-right is computed, combining a point-to-all nucleon two-point function with a stochastically estimated meson two-point function, using the “one-end-trick” [35–37]. For the quark-line connected diagrams, we use the sequential source method [34] to compute the all-to-all propagators. The Wick contractions for the two-point functions Eq. (S3) have the same topologies and are computed in a similar way, replacing the current by a smeared pion interpolating operator at  $\tau = 0$ .



Most computer time is spent on the quark-line connected diagrams, where we employ the sequential-source method twice for each combination of momentum projections at  $y$  and at  $x^1$  as well as for each spin polarization of  $O_{3q}$ . The disconnected diagram is much less expensive. The total cost for each nucleon source position and fixed source-sink separation on a given configuration is equivalent to the computation of about 200 propagators. This

can be compared to three propagators for the standard three-point function, when setting  $\mathbf{p}' = \mathbf{0}$  and considering the unpolarized case and one polarization. Including  $\mathbf{p}' = \pm \mathbf{e}_i$  (as we do here) increases this cost five-fold (15 propagators) and there would be an additional factor if further polarizations were evaluated. Therefore, the addition of the  $O_{5q}$  interpolators increases the computational complexity by about one order of magnitude.

- 
- [1] Y. Fukuda *et al.* (Super-Kamiokande), Evidence for oscillation of atmospheric neutrinos, *Phys. Rev. Lett.* **81**, 1562 (1998), arXiv:hep-ex/9807003.
- [2] Q. R. Ahmad *et al.* (SNO), Measurement of the rate of  $\nu_e + d \rightarrow p + p + e^-$  interactions produced by  $^8\text{B}$  solar neutrinos at the Sudbury Neutrino Observatory, *Phys. Rev. Lett.* **87**, 071301 (2001), arXiv:nucl-ex/0106015.
- [3] M. A. Acero *et al.* (NOvA), Improved measurement of neutrino oscillation parameters by the NOvA experiment, *Phys. Rev. D* **106**, 032004 (2022), arXiv:2108.08219 [hep-ex].
- [4] K. Abe *et al.* (T2K), Constraint on the matter–antimatter symmetry-violating phase in neutrino oscillations, *Nature* **580**, 339 (2020), [Erratum: *Nature* 583, E16 (2020)], arXiv:1910.03887 [hep-ex].
- [5] B. Abi *et al.* (DUNE), Deep Underground Neutrino Experiment (DUNE), far detector technical design report, volume I introduction to DUNE, *JINST* **15** (08), T08008, arXiv:2002.02967 [physics.ins-det].
- [6] J. Bian *et al.* (Hyper-Kamiokande), Hyper-Kamiokande experiment: a Snowmass white paper, in *2022 Snowmass Summer Study* (2022) arXiv:2203.02029 [hep-ex].
- [7] C. Andreopoulos *et al.* (GENIE), The GENIE neutrino Monte Carlo generator, *Nucl. Instrum. Meth. A* **614**, 87 (2010), arXiv:0905.2517 [hep-ph].
- [8] J. Tena-Vidal *et al.* (GENIE), Neutrino-nucleon cross-section model tuning in GENIE v3, *Phys. Rev. D* **104**, 072009 (2021), arXiv:2104.09179 [hep-ph].
- [9] J. A. Formaggio and G. P. Zeller, From eV to EeV: neutrino cross sections across energy scales, *Rev. Mod. Phys.* **84**, 1307 (2012), arXiv:1305.7513 [hep-ex].
- [10] B. Märkisch *et al.*, Measurement of the weak axial-vector coupling constant in the decay of free neutrons using a pulsed cold neutron beam, *Phys. Rev. Lett.* **122**, 242501 (2019), arXiv:1812.04666 [nucl-ex].
- [11] V. A. Andreev *et al.* (MuCap), Measurement of muon capture on the proton to 1% precision and determination of the pseudoscalar coupling  $g_P$ , *Phys. Rev. Lett.* **110**, 012504 (2013), arXiv:1210.6545 [nucl-ex].
- [12] A. S. Meyer, A. Walker-Loud, and C. Wilkinson, Status of lattice QCD determination of nucleon form factors and their relevance for the few-GeV neutrino program, *Annu. Rev. Nucl. Part. Sci.* **72**, 205 (2022), arXiv:2201.01839 [hep-lat].
- [13] D. Simons, N. Steinberg, A. Lovato, Y. Meurice, N. Rocco, and M. Wagman, Form factor and model dependence in neutrino-nucleon cross section predictions, (2022), arXiv:2210.02455 [hep-ph].
- [14] G. S. Bali, L. Barca, S. Collins, M. Gruber, M. Löffler, A. Schäfer, W. Söldner, P. Wein, S. Weishäupl, and T. Wurm (RQCD), Nucleon axial structure from lattice QCD, *J. High Energy Phys.* **05**, 126, arXiv:1911.13150 [hep-lat].
- [15] Y.-C. Jang, R. Gupta, B. Yoon, and T. Bhattacharya, axial vector form factors from lattice QCD that satisfy the PCAC relation, *Phys. Rev. Lett.* **124**, 072002 (2020), arXiv:1905.06470 [hep-lat].
- [16] C. Alexandrou *et al.* (ETM), Nucleon axial and pseudoscalar form factors from lattice QCD at the physical point, *Phys. Rev. D* **103**, 034509 (2021), arXiv:2011.13342 [hep-lat].
- [17] S. Park, R. Gupta, B. Yoon, S. Mondal, T. Bhattacharya, Y.-C. Jang, B. Joó, and F. Winter (NME), Precision nucleon charges and form factors using (2+1)-flavor lattice QCD, *Phys. Rev. D* **105**, 054505 (2022), arXiv:2103.05599 [hep-lat].
- [18] D. Djukanovic, G. von Hippel, J. Koponen, H. B. Meyer, K. Ottnad, T. Schulz, and H. Wittig, Isovector axial form factor of the nucleon from lattice QCD, *Phys. Rev. D* **106**, 074503 (2022), arXiv:2207.03440 [hep-lat].
- [19] A. S. Meyer, M. Betancourt, R. Gran, and R. J. Hill, Deuterium target data for precision neutrino-nucleus cross sections, *Phys. Rev. D* **93**, 113015 (2016), arXiv:1603.03048 [hep-ph].
- [20] G. S. Bali, S. Collins, B. Glässle, M. Göckeler, J. Najjar, R. H. Rödl, A. Schäfer, R. W. Schiel, W. Söldner, and A. Sternbeck (RQCD), Nucleon isovector couplings from  $N_f = 2$  lattice QCD, *Phys. Rev. D* **91**, 054501 (2015), arXiv:1412.7336 [hep-lat].
- [21] S. Capitani, M. Della Morte, D. Djukanovic, G. M. von Hippel, J. Hua, B. Jäger, P. M. Junnarkar, H. B. Meyer, T. D. Rae, and H. Wittig, Isovector axial form factors of the nucleon in two-flavor lattice QCD, *Int. J. Mod. Phys. A* **34**, 1950009 (2019), arXiv:1705.06186 [hep-lat].
- [22] R. Gupta, Y.-C. Jang, H.-W. Lin, B. Yoon, and T. Bhattacharya (PNDME), Axial vector form factors of the nucleon from lattice QCD, *Phys. Rev. D* **96**, 114503 (2017), arXiv:1705.06834 [hep-lat].
- [23] N. Tsukamoto, K.-I. Ishikawa, Y. Kuramashi, S. Sasaki, and T. Yamazaki (PACS), Nucleon structure from 2 + 1 flavor lattice QCD near the physical point, *EPJ Web Conf.* **175**, 06007 (2018), arXiv:1710.10782 [hep-lat].
- [24] G. S. Bali, S. Collins, M. Gruber, A. Schäfer, P. Wein, and T. Wurm (RQCD), Solving the PCAC puzzle for nucleon axial and pseudoscalar form factors, *Phys. Lett. B* **789**, 666 (2019), arXiv:1810.05569 [hep-lat].
- [25] O. Bär,  $N\pi$ -state contamination in lattice calculations of

---

<sup>1</sup> We use  $\mathcal{D}^{-1}(x, z)\gamma_5\mathcal{D}^{-1}(z, x)\gamma_5$  (and the same for  $\mathcal{D}^{-1}(x, y)$ ). Some building blocks are shared between different diagrams.

- the nucleon axial form factors, *Phys. Rev. D* **99**, 054506 (2019), arXiv:1812.09191 [hep-lat].
- [26] O. Bär,  $N\pi$ -state contamination in lattice calculations of the nucleon pseudoscalar form factor, *Phys. Rev. D* **100**, 054507 (2019), arXiv:1906.03652 [hep-lat].
  - [27] O. Bär,  $N\pi$  states and the projection method for the nucleon axial and pseudoscalar form factors, *Phys. Rev. D* **101**, 034515 (2020), arXiv:1912.05873 [hep-lat].
  - [28] B. C. Tiburzi, Chiral corrections to nucleon two- and three-point correlation functions, *Phys. Rev. D* **91**, 094510 (2015), arXiv:1503.06329 [hep-lat].
  - [29] M. T. Hansen and H. B. Meyer, On the effect of excited states in lattice calculations of the nucleon axial charge, *Nucl. Phys. B* **923**, 558 (2017), arXiv:1610.03843 [hep-lat].
  - [30] L. A. Ruso *et al.*, Theoretical tools for neutrino scattering: interplay between lattice QCD, EFTs, nuclear physics, phenomenology, and neutrino event generators, (2022), arXiv:2203.09030 [hep-ph].
  - [31] M. Göckeler, R. Horsley, M. Lage, U. Meißner, P. E. L. Rakow, A. Rusetsky, G. Schierholz, and J. M. Zanotti, Scattering phases for meson and baryon resonances on general moving-frame lattices, *Phys. Rev. D* **86**, 094513 (2012), arXiv:1206.4141 [hep-lat].
  - [32] C. B. Lang, L. Leskovec, M. Padmanath, and S. Prelovsek, Pion-nucleon scattering in the Roper channel from lattice QCD, *Phys. Rev. D* **95**, 014510 (2017), arXiv:1610.01422 [hep-lat].
  - [33] S. Prelovsek, U. Skerbis, and C. B. Lang, Lattice operators for scattering of particles with spin, *J. High Energy Phys.* **01**, 129, arXiv:1607.06738 [hep-lat].
  - [34] L. Maiani, G. Martinelli, M. L. Paciello, and B. Taglienti, Scalar densities and baryon mass differences in lattice QCD with Wilson fermions, *Nucl. Phys. B* **293**, 420 (1987).
  - [35] R. Sommer, Leptonic decays of  $B$  and  $D$  mesons, *Proceedings, 12th International Symposium on Lattice Field Theory (Lattice 94), Bielefeld, Germany, September 27–October 1, 1994*, *Nucl. Phys. Proc. Suppl.* **42**, 186 (1995), arXiv:hep-lat/9411024 [hep-lat].
  - [36] M. Foster and C. Michael (UKQCD), Hadrons with a heavy color adjoint particle, *Phys. Rev. D* **59**, 094509 (1999), arXiv:hep-lat/9811010 [hep-lat].
  - [37] M. Foster and C. Michael (UKQCD Collaboration), Quark mass dependence of hadron masses from lattice QCD, *Phys. Rev. D* **59**, 074503 (1999).
  - [38] M. Bruno *et al.* (CLS), Simulation of QCD with  $N_f = 2 + 1$  flavors of non-perturbatively improved Wilson fermions, *J. High Energy Phys.* **02**, 043, arXiv:1411.3982 [hep-lat].
  - [39] G. S. Bali, S. Collins, P. Georg, D. Jenkins, P. Korcyl, A. Schäfer, E. E. Scholz, J. Simeth, W. Söldner, and S. Weishäupl (RQCD), Scale setting and the light baryon spectrum in  $N_f = 2 + 1$  QCD with Wilson fermions, (2022), arXiv:2211.03744 [hep-lat].
  - [40] B. Berg, Glueball calculations in lattice gauge theories, *J. Phys. Colloq.* **43**, 272 (1982).
  - [41] C. Michael, Adjoint sources in lattice gauge theory, *Nucl. Phys. B* **259**, 58 (1985).
  - [42] M. Lüscher and U. Wolff, How to calculate the elastic scattering matrix in two-dimensional quantum field theories by numerical simulation, *Nucl. Phys. B* **339**, 222 (1990).
  - [43] B. Blossier, M. Della Morte, G. von Hippel, T. Mendes, and R. Sommer, On the generalized eigenvalue method for energies and matrix elements in lattice field theory, *J. High Energy Phys.* **04**, 094, arXiv:0902.1265 [hep-lat].
  - [44] J. Bulava, M. Donnellan, and R. Sommer, On the computation of hadron-to-hadron transition matrix elements in lattice QCD, *J. High Energy Phys.* **01**, 140, arXiv:1108.3774 [hep-lat].
  - [45] B. J. Owen, J. Dragos, W. Kamleh, D. B. Leinweber, M. S. Mahbub, B. J. Menadue, and J. M. Zanotti, Variational approach to the calculation of  $g_A$ , *Phys. Lett. B* **723**, 217 (2013), arXiv:1212.4668 [hep-lat].
  - [46] J. Dragos, R. Horsley, W. Kamleh, D. B. Leinweber, Y. Nakamura, P. E. L. Rakow, G. Schierholz, R. D. Young, and J. M. Zanotti, Nucleon matrix elements using the variational method in lattice QCD, *Phys. Rev. D* **94**, 074505 (2016), arXiv:1606.03195 [hep-lat].
  - [47] J. Liang, Y.-B. Yang, K.-F. Liu, A. Alexandru, T. Draper, and R. S. Sufian ( $\chi$ QCD), Lattice calculation of nucleon isovector axial charge with improved currents, *Phys. Rev. D* **96**, 034519 (2017), arXiv:1612.04388 [hep-lat].
  - [48] Jülich Supercomputing Centre, JURECA: modular supercomputer at Jülich Supercomputing Centre, *J. of large-scale research facilities* **4**, A132 (2018).
  - [49] R. G. Edwards and B. Joó (SciDAC, LHP and UKQCD), The Chroma software system for Lattice QCD, *Nucl. Phys. B Proc. Suppl.* **140**, 832 (2005), arXiv:hep-lat/0409003 [hep-lat].